A shear wave analysis system for semi-automatic measurements of shear wave splitting above volcanic earthquakes: descriptions and applications

L. Zaccarelli and F. Bianco

Istituto Nazionale di Geofisica e Vulcanologia, sezione di Napoli

Abstract
Our interest is the study of the seismograms with the purpose of monitoring and modelling volcanoes. In particular, since the shear waves bring information about the anisotropic system characterizing the shallow crust, they are also sensitive to all temporal variations caused by changes in the stress field acting on the area. Therefore we intend to realize an algorithm that can provide shear wave splitting estimates in quasi-real time and in a semi-automatic way. Finally we perform validation tests on both real and synthetic data, in order to define the accuracy and validity range of our program.

Introduction
A transverse wave that enters an anisotropic volume is split into two *quasi*-waves showing perpendicular polarizations and travelling with different velocities. This phenomenon, known as birefringence in optics, is called Shear-Wave Splitting in seismology. It can be detected and well described directly from the seismograms, through the estimation of two parameters: the faster S-wave polarization direction ϕ, and the time delay T_d between the two S-waves. At crustal scale, the more common source of seismic anisotropy is the presence of preferentially oriented heterogeneities and (micro)cracks in the rock, whose orientation comes from the stress field acting on the area. In this framework, azimuth ϕ, expressed in degrees from the N, will be parallel to the maximum compressive stress. Time delays, instead, are related to the characteristics of the crack system inside the anisotropic volume, as well as its extension along the ray path. This dependency varies with the incidence angle at the seismic station, distinguishing 2 bands inside a solid angle that ensures no interference with the free surface. The cone of incidences, named Shear Wave Window (SWW), depends on v_p/v_s ratio, and extends until 35° from the vertical for crustal rocks. Between 0 and 15° T_d values are symptomatic of the microcrack density -*Band2*-, from 15 to 35° T_d is affected by their aspect ratio -*Band1*- (Crampin and Chastin, 2003 and references therein). In this picture the two splitting parameters are more or less directly linked to the stress field and can be considered as an interesting tool for monitoring purpose describing not only the features of the stress field but even their temporal variations.

Volcanic stress monitoring
When a volcanic area is interested by an impending eruption, some amount of magma rises from depth to the surface producing an increasing pressure on the surrounding rocks. This almost vertical stress change cause a variation in both crack density and aspect-ratio, if the upper crust is pervaded by fluid filled stress aligned microcracks. Indeed, cracks laying perpendicular to the stress variation tend to close while those parallel grow rounding their shape. The consequences in terms of time delays are that T_d values decrease in *Band2*, in opposition with those increasing in *Band1*. If the stress intensity is augmenting more and more, then it will join the system criticality. Such an overpressurized regime is visible through the 90°-flip of ϕ: the two *quasiS*-waves interchange their polarization directions. From this moment the system can fail for even a small perturbation and then the eruption may start. Its occurrence is accompanied by a stress relaxation in the area, that will produce an inversion in time delay temporal variations. All these phenomena are explained by the APE -Anisotropic Poro Elasticity- theoretical model (Zatsepin and Crampin, 1997; Crampin and Zatsepin, 1997) and have been observed in volcanic regions before eruptions such as Ruapehu (Gerst and Savage, 2004), Etna (Bianco et al. 2006), and before a major earthquake at Mt. Vesuvius (Del Pezzo et al., 2004).
This framework highlights the importance of developing the splitting parameter estimation in a (semi)automatic way and quasi-real time.

SPY: Splitting Parameter Yield

Semi-automatic algorithm

Automation means any user can deal with a faster and easier tool, able to process a big amount of data at a time. We chosen a semi-automatic procedure in order to avoid as much as possible the fluctuations due to subjectivity with no reduction in terms of estimate accuracy. Actually, the picking phase loses in precision if not executed by an expert eye, especially when we are looking for shear wave arrival inside a volcanic event seismogram. The first step of our approach is therefore a manual resolution of P and S times, whose determination is usually made together with the event location process. Then it starts the automation stage: a program written in Matlab, that is a versatile and user-friendly environment.

Command line >> spy(*directory*)
Being *directory* the complete path where the data files are stored.

Input The hypocenter locations of the events and the coordinates of all seismic stations both in km (UTM). The 2 file paths have to be set in advance directly in the code. Finally, the 3-component seismograms, and P and S arrival times organized in sub-directories per each earthquake or station inside the *directory* given in the command line.

Options

Data file format: '*SAC*' / '*ASCII*' (To be set in the code)
Depending on the file format, the program will get the time information from the sac header or from a picking file, whose extension is ".pick" by default.

Plots: '*Y*' / '*N*' (To be set in the code)
If the plot option has been set to 'Y', then during execution, the horizontal components of each event will be plotted either before and after rotation along the polarization direction found. This is a way to visually check the goodness of the results as well as the optional parameters, useful especially when the signal characteristics are unknown.

Shear Wave Window: '*y*'$\rightarrow$ *Band* / '*n*'$\rightarrow$ *[i_1 i_2]* (Running the program request)
Here we can choose the incidence angles to be considered: Band can be 1 or 2, inside the shear wave window ([0; 35]°) or a different Band can be defined inserting [i_1;i_2] in degrees.

Resampling: '*y*' / '*n*' (Running the program request)
To be careful in manipulating the data, but if necessary the sampling rate can be doubled through the spline algorithm.

Filtering: '*y*'$\rightarrow$ *[f_1 f_2]* / '*n*' (Running the program request)
In case of very high noise, it is possible to clean the data through a filter, by default a Butterworth bandpass 1-pole, 0-phase with corner frequencies from input. This option is even more delicate and controversial than the previous one, therefore it would be appropriate to verify the stability of the results changing the interval [f_1;f_2].

Cross-correlation threshold: *value* (Running the program request)
Setting a threshold value $\subset$ [0;1[for the similarity of the 2 components.

Algorithm

There exists many different techniques to calculate the splitting parameters and all of them presents weakness as well as strength points (Crampin and Gao, 2006). Our choice was leaded by reducing to minimum the user intervention during the analysis.

ϕ estimate The program takes a signal portion starting with the S picking, and ideally ending before the qS_2 arrival time. This time window is the only value that needs to be previously defined by the operator because strongly depends on the signal characteristics. Anyway, the delay between the 2 *quasi*-waves is not known yet, therefore it is convenient to run the program with a first guess, then to adjust the value of the window with the resulting T_d. This feed-back process has been functional even to study the variability of the outcomes versus the length of the sub-dataset under analysis. From this portion of seismogram it is calculated the covariance matrix, whose elements are indicators of the relationship between each component. The covariance diagonalization defines a new coordinate system where the horizontal E and N components would become qS_1 and qS_2. Hence, the fast polarization direction can be found through the azimuth defined by the eigenvector corresponding to the maximum eigenvalue. ϕ angle is estimated in degrees from the N and its value is positive and less then 180°.

T_d estimate Firstly the 3 seismogram traces have been rotated in the ϕ direction, obtaining the new decomposition in fast, slow, and everything else components. For the evaluation of the time delay we opted for the cross correlation methodology: a comparison of the two split waves that measures their similarity versus a shift in time. Again, we need to extract a portion of signal starting from the S-wave arrival and lasting for no less than a period but not too much beyond it, in order to compare only the 2 quasi-waves without other seismic phases. This time we could automatically determine the length of the time window through the estimate of the predominant frequency inside 3 seconds of data from the P arrival time. The more energetic part of the spectrum, indeed, is due to the shear waves. Basically, the program operates a FFT algorithm on the data, and from that, it calculates the frequency at which the power spectrum reaches its maximum value. The period corresponding to the proper frequency found marks the end of the signal portion for the following step. The cross correlation function of fast and slow components would join its maximum for a sample lag that, multiplied by the sampling rate gives the delay sought (in seconds). To refine the evaluation of this time lag, we resampled the function in the proximity of its maximum value, obtaining a more precise time resolution. This operation is not adding further uncertainties because of the smoothly property of the cross correlation function (VanDecar and Crosson, 1990).

Statistics In a further stage of the analysis, only those outcomes that meet all requirements defined in the options are considered for statistical manipulations. Moreover the events with a T_d=0 have to be discarded, because it can be symptom of no anisotropic volume or, more easily, of a mistaken value. The errors on polarization directions are estimated as standard deviation over more circular data (Mardia and Jupp, 2000), preferentially referring to the same station records. Errors associated to time delays, instead, come from the procedure used, and are equal to 1/2 sampling rate for all earthquakes, since the resolution of the refined cross correlation function is half sample. We finally calculate the normalized time delays, dividing any T_d by its related hypocenter distance. These values are helpful for a comparison among events, under the assumption that all ray paths are sampling almost the same anisotropic volume. This hypothesis is not too strong, especially working on volcanic events that normally occur inside a small volume. In any case T_n is a helpful measure, even if not completely disconnected by location effects. Its error is defined by the propagation formula:

$$T_n = T_d/D \quad \Longrightarrow \quad \delta T_n = \frac{\sqrt{\delta T_d^2 + T_n^2 \cdot \delta D^2}}{D} \qquad \text{(Eq.1)}$$

Where D is the hypocenter distance to the seismic station, and with δ are indicated all error estimates. It is worthy to note the dependency of this value accuracy on the precisions of both time delays and locations.

Output The program save two kinds of Matlab variables (".mat") for each subdirectory found in the input data path *directory*, i.e. for any station or event, established on how the data have been grouped and stored. Variable names are by default "swsSUB.mat" and "tdSUB.mat" where SUB stands for (and will be replaced by) subdirectory name.

swsSUB.mat The first variable saves all rough results obtained by running the program. If loaded, it will appear as a matrix composed by a line for each record found in SUB, per 6 columns. The column meanings are, respectively: incidence angle (°); D (km); P time (s); ϕ (°N); cross correlation maximum value; and T_d (s). When the event record is out of bound (out of allowed incidences, or cross correlation threshold), it is assigned a fake value of 1000 or -9 to all cells.

tdSUB.mat This second matrix is composed by as many lines as the selected events inside the incidence cone, with cross correlation maximum greater than the similarity threshold, and whose time delay estimate is not zero. The 5 columns report time of the P wave (s); T_n (s/km); δT_n (s/km); ϕ (°N); σ_ϕ (°).

Applications

SPY program has been tested and calibrated through the analysis of both real and synthetic data.

Real data: Etna 2002

We had availability of seismograms recorded at Mt. Etna during the 2002-2003 fissure eruption. This events were not yet studied, but we could compare our results with those coming from

previous works on Etna seismicity and its splitting parameter evaluations (Bianco et al, 2006). In general SPY outcomes are in agreement with those reported in literature, showing a roughly E-W mean polarization, 90°-flipped with respect to the regional stress direction (Musumeci at al, 2004); and small T_n values (of the order of few ms per km). Anyway a more detailed interpretation of the results is complicated by the great instability due to the ongoing eruption, and need further studies. In the present report we highlight the importance of the parameter set calibration phase through this practical example over real data. In particular, we tested the stability of the results in changing the covariance matrix time window length τ. As already described in the ϕ estimate paragraph, this window has to be ideally long as the time delay we are looking for. Starting from the qS_1 arrival time and lasting till the qS_2.

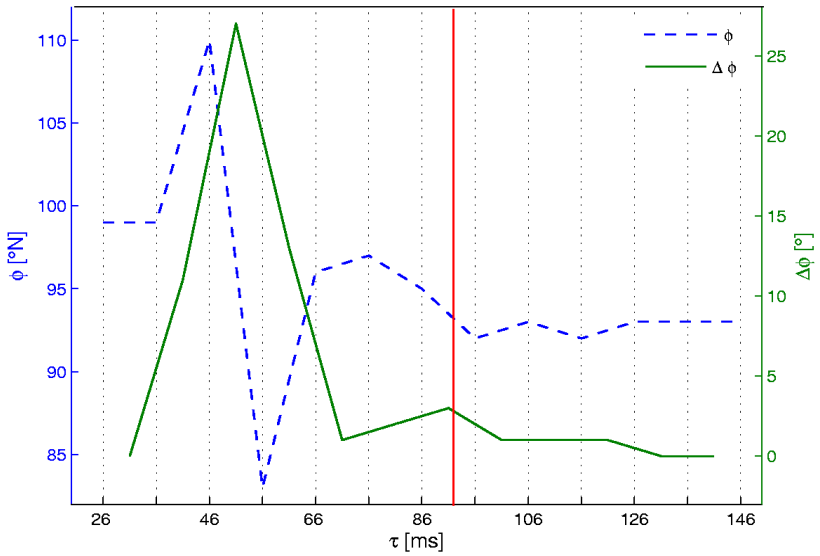

Figure 1 – ϕ measures (dashed line, y-axis on the left) and their variations $\Delta\phi$ calculated over subsequent values (straight segments, right y-axis), versus length of the time window used, τ. Beyond the vertical line the window is certainly taking some portion of qS_2 wave.

Figure 1 reports in dashed line the mean polarization directions over all events in the SWW at one station (ERCB, the closest to the hypocenter locations), while the straight segments outline the azimuthal difference between successive points. The lines draw the behaviour of this 2 measures versus increasing τ from 0.026 s to 0.146 s, at constant steps of 10 ms. The window has a starting point fixed at the S picking time minus 2 samples (=0.016 s) to ensure the beginning of the shear wave lay inside the signal portion considered. For all trials we found time delays less than 0.092 s, marked with the vertical line, that hence become an upper limit for τ length. We are interested in points where the results are almost stable (Teanby et al., 2004), meaning that the covariance matrix is well defined, i.e. compound by enough data, before the slower wave arrival. In our case we can see big oscillations of ϕ in the first τ guesses, than a *plateau* is reached right before the boundary vertical line. Therefore we selected a window length of 0.076 s as the more plausible and accurate for these seismograms.

Synthetic data

The OGS group (Klin et al.) provided us with 3 synthetic events at Campi Flegrei, recorded by 13 seismic stations: ASE, ASO, BAC, DMP, NIS, O04, O14, O29, W03, W11, W12, W15, W20. The three simulations share the same epicenter coordinates but associate them three different depths, respectively: -1.7; -3.4; and -5.4 km. Each synthetic event is in form of a single sac file per component at any station. Figure 2a shows the horizontal projection of stations (blue triangles) and epicenter location (red asterisk) with the black curve marking the Campi Flegrei coast line, the inland on the upper part and the sea on the bottom. In figure 2b is a vertical projection of stations and hypocenter locations together with a simplified sketch of the velocity model used for generating the simulations. The model is quite complex with only one isotropic layer, the shallower, from the surface down to -0.6 km with P velocity increasing linearly with depth from 2.5 to 3 km/s and v_p/v_s = 2.5. The second layer extends from 0.6 till 1-1.5 km under the surface (the bottom floor being not planar), its v_p reaches the 3.9 km/s at depth, and v_p/v_s ratio is 2. Then it starts another layer that goes down until a variable depth of -4.5/-5.5 km where v_p has its maximum value of 5.4 km/s, while, as before, v_p/v_s is constantly 1.8. Finally there is a half-space characterized by v_p=6.5 km/s and v_p/v_s=1.699.

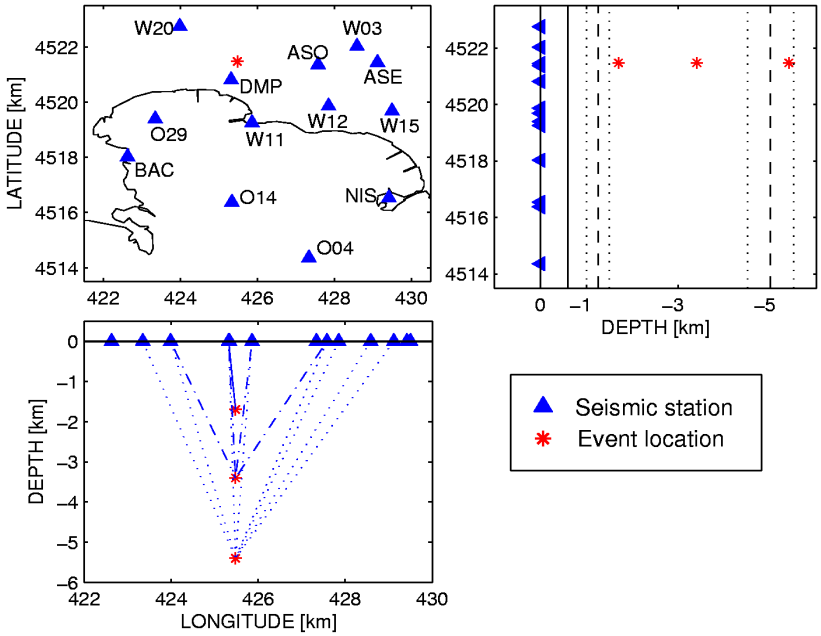

Figure 2 – Hypocenter and seismic station distributions, in UTM coordinates, for the synthetic experiments. a) Horizontal projection with Campi Flegrei coast line. b) Latitude versus depth where the vertical lines sketch the 4 layers compounding the velocity model: dotted lines evidence the depth range where the boundary can extend, with the dashed one in the middle for non planar separation mean depth. c) Depth versus longitude. The three events are linked to those stations laying inside their SWW (35° cone).

Below the first 600 m, all layers are thought as pervaded by a Shear Wave velocity Anisotropy swa=10% with symmetry axis parallel to the EW direction. From this velocity model we have extrapolated a mean S-wave velocity averaging over all central v_s values weighted with the corresponding mean thickness of the i^{th} layer:

$$\overline{v}_s = \sum_{i}^{3} \overline{v}_{s_i} \cdot \overline{h}_i \,/\, \overline{H} = 2.3 \text{ km/s}\,; \qquad \overline{H} = 5 \text{ km} \qquad \text{(Eq.2)}$$

Following Savage et al., 1990, we combined this mean value with T_d estimated by SPY to obtain the shear wave anisotropy percentage (swa in equation 3), in order to make a comparison with the theoretical one.

$$\text{swa} = \left(\frac{\overline{T}_d}{\overline{D}} \cdot \overline{v}_s \right) \cdot 100\,; \qquad \text{(Eq.3)}$$

$\overline{T}_d$, $\overline{D}$ averaged over all station records

In table 1 we report SPY measurements only for those seismic stations positioned in the shear wave window with respect to the simulation hypocenters (see also figure 2c).

station	i [°]	D [km]	ϕ [°N]	T_d [s]	swa [%]	
DMP	22	1.8	109	0.005	0.6	TEST 1
ASO	32	4.0	88	0.06	3	
DMP	11	3.5	1	0.15	10	
W11	34	4.1	2	0.12	7	TEST 2
W20	30	3.9	173	0.035	2	
ASE	34	6.5	86	0.06	2	
ASO	21	5.8	89	0.08	3	
DMP	7	5.4	106	0.035	1.5	
O29	29	6.2	92	0.21	8	
W03	30	6.3	159	0.065	2	TEST 3
W11	23	5.9	83	0.255	10	
W12	28	6.1	85	0.035	1	
W20	20	5.7	107	0.205	8	

Table 1 – Results for the three synthetic events recorded at stations where they had an incidence angle inside the shear wave window. The columns report: station name, incidence angle, hypocentral distance, fast polarization direction, time delay, anisotropy percentage.

Test 1 is the synthetic event with depth -1.7 km. Only DMP is inside the 35° cone of incidence. The qS_1 polarization direction is a little bit more than the theoretical 90° (fig. 3a) and swa calculated is almost 0.
The deeper source at -3.4 km (test 2) increases to 4 the number of stations inside SWW. The right ϕ direction has been detected only at ASO (see fig. 3b), whilst swa is 10% only for DMP. We are searching for possible reasonable explanations for the spurious ϕ measurements obtained in this second simulation at W11, DMP, and W20 stations; actually we are exploiting the possibility that qS_1 polarization may be corrupted by the presence of irregular interfaces near the source.
Last test hypocenter is located 5.4 km down from the surface. The stations viewed with an angle less than 35° are 8. All of them show a ϕ EW oriented excepted W03 (figure 3c), anyway only 3 (O29, W11, W20) time delays can produce a percentage anisotropy close to the 10%.

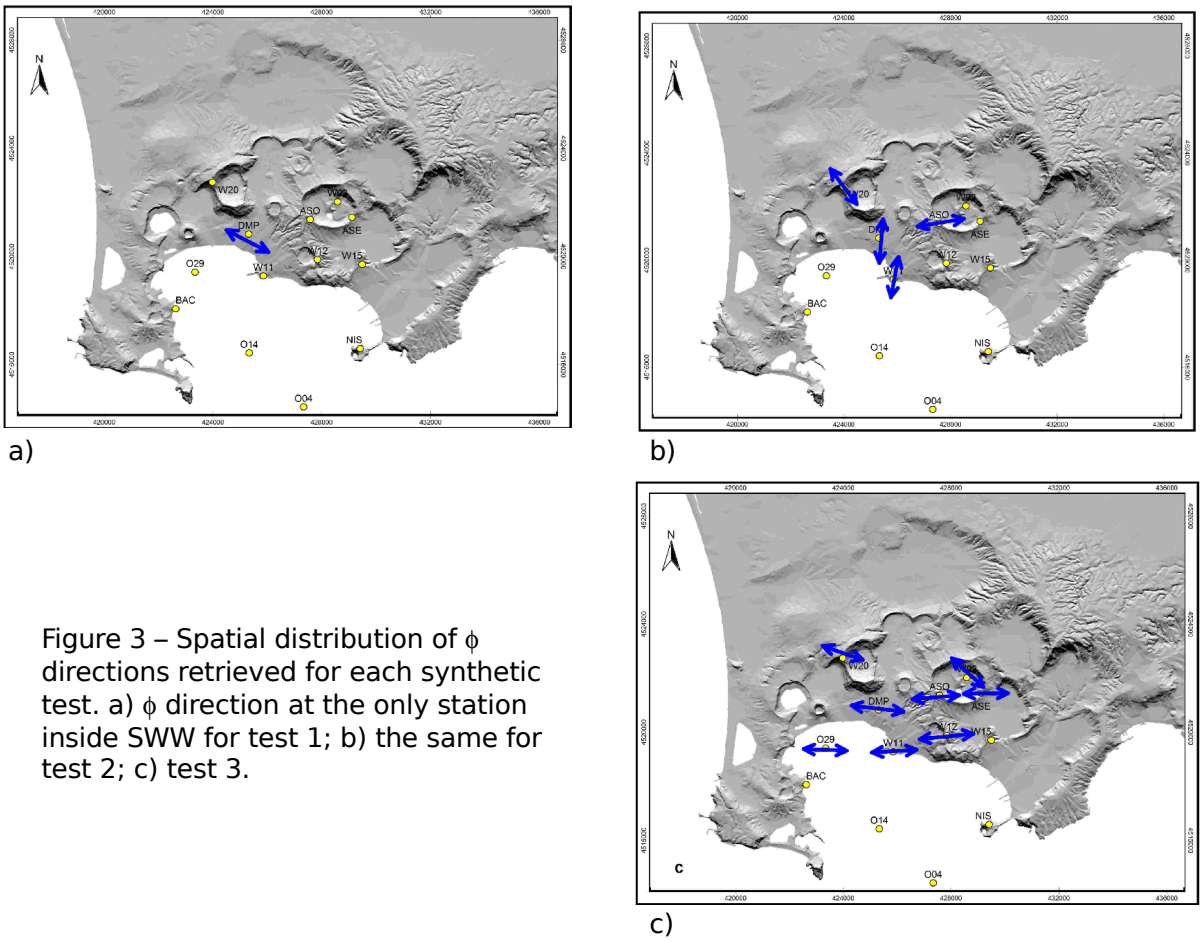

Figure 3 – Spatial distribution of ϕ directions retrieved for each synthetic test. a) ϕ direction at the only station inside SWW for test 1; b) the same for test 2; c) test 3.

This disagreement can be ascribed to swa index we calculate that is not properly the same intended in the crustal model, since the splitting of the shear wave depends on both aspect ratio and density of microcracks, while the percentage used to build up the synthetic traces is a measure of the number of cracks inside the surrounding rock, independently from their volume. Moreover, equation 3 refers to averaged value over multiple records, meaning that we would need various simulated events to gain significance and accuracy in swa estimate. The interesting found is the right estimate of fast polarization direction. Even when we look at all records, independently from the incidence angle, the mean value is correctly around 90°.

Conclusions

We developed a semi-automatic algorithm able to yield shear wave splitting parameter estimates in quasi-real time. The final aim would be to exploit them as an additional and useful tool for monitoring temporal variations in the stress field acting on volcanic areas. The program has been tested through the analysis of both real and synthetic data. Results coming from 2002 eruption on Etna are completely in agreement with previous measurements. Furthermore the real data have been used to verify the capability in the feedback process to evaluate the correct parameter set or the validity range for the input choices (such as filtering and resampling

operations). The analysis of synthetic data is an entirely unexplored field in terms of anisotropic system. We applied our algorithm to three simulated events with different depths, obtaining averaged values that can reproduce the underlying theoretical model, adding an independent validation of our program.

References

Bianco F., L. Scarfì, E. Del Pezzo, and D. Patanè (2006). Shear wave splitting changes associated with the 2001 volcanic eruption on Mt Etna. *Geophys. J. Int.* **167**, 959-967.

Crampin S., and S. V. Zatsepin (1997). Modeling the compliance of crustal rock-II. Response to temporal changes before earthquakes. *Geophys. J. Int.* **129**, 495-506.

Crampin, S. (1999). Calculable fluid-rock interactions. *J. Geol. Soc.* **156**, 501-512.

Crampin S., and S. Chastin (2003). A review of shear wave splitting in the crack-critical crust. *Geophys. J. Int.* **155**, 221-240.

Crampin S. and Y. Gao (2006). A review of techniques for measuring shear-wave splitting above small earthquakes. *Phys. Earth Planet. Interiors* **159**, 1-14.

Del Pezzo E., F. Bianco, S. Petrosino, and G. Saccorotti (2004). Changes in coda decay rate and shear-wave splitting parameters associated with seismic swarms at Mt. Vesuvius, Italy. *Bull. Seism. Soc. Am.* **94**, 2, 439-452.

Gerst A., and M. Savage (2004). Seismic Anisotropy Beneath Ruapehu Volcano: A Possible Eruption Forecasting Tool. *Science* **306**, 1543-1547.

Mardia K.V., and P.E. Jupp (2000). Directional statistics. Ed.Wiley and Sons Ltd.

Musumeci C., O. Cocina, P. De Gori, D. Patanè (2004). Seismological evidence of stress induced by dike injection during the 2001 Mt. Etna eruption. *Geophys. Res. Lett.* **31**, L07617, doi:10.1029/2003GL019367.

Savage M.K., W.A. Peppin, and U.R. Vetter (1990). Shear wave anisotropy and stress direction in and near the Long Valley caldera, California, 1979/1988. *J. Geophys. Res.* **95**, 11,165-11,177.

Teanby N.A., J.M. Kendall, and M. van der Baan (2004). Automation of shear-wave splitting measurements using cluster analysis. *Bull. Seism. Soc. Am.* **94**, 2, 453-463.

VanDecar J.C., and R.S. Crosson (1990). Determination of teleseismic relative phase arrival time using multi-channel cross-correlation and least squares. *Bull. Seism. Soc. Am.* **80**, 1, 150-169.

Zatsepin S. V., and S. Crampin (1997). Modeling the compliance of crustal rock-I. Response of shear-wave splitting to differential stress. *Geophys. J. Int.* **129**, 477-494.